Heliyon 10 (2024) e30926

Contents lists available at ScienceDirect

Heliyon

journal homepage: www.cell.com/heliyon

Research article

Comparative study of TDDFT and TDDFT-based STEOM-DLPNO-CCSD calculations for predicting the excited-state properties of MR-TADF

Sunwoo Kang [a,**], Taekyung Kim [b,c,*]

[a] Department of Chemistry, Dankook University, Cheonan, Chungnam, 31116, South Korea
[b] Department of Materials Science and Engineering, Hongik University, Sejongsi, 30016, South Korea
[c] Department of Information Display Engineering, Hongik University, Seoul, 04066, South Korea

ARTICLE INFO

Keywords:
Density functional theory
STEOM-DLPNO-CCSD
Correlation effect
MR-TADF
Excited-state properties

ABSTRACT

The time dependent density functional theory (TDDFT) and TDDFT/similarity transformed EOM domain-based local pair natural orbital CCSD (STEOM-DLPNO-CCSD) calculations were explored to estimate their validity in predicting the excited-state properties of multi-resonant thermally activated delayed fluorescence (MR-TADF) materials. Obviously, it was demonstrated that TDDFT calculation is inadequate to provide the quantitative prediction of the lowest singlet excited-state (S_1), the lowest triplet excited-state (T_1), and ΔE_{ST}. On the other hand, TDDFT/STEOM-DNLPNO-CCSD calculation reveals the superior prediction of S_1, T_1, and ΔE_{ST} that are in quantitative agreement with experiments. More importantly, it was found that TD-LC-]*HPBE/STEOM-DLPNO-CCSD calculation provides the most accurate prediction of S_1, T_1, and ΔE_{ST}. Accordingly, we suggest that TD-LC-]*HPBE/STEOM-DLPNO-CCSD calculation should be utilized to compute the excited-states properties of MR-TADF materials accurately.

1. Introduction

Since the first report by Hatakeyama et al. [1], the multi-resonant thermally activated delayed fluorescence (MR-TADF) materials, which exhibit the short-range intramolecular charge transfer and double excitation characteristics, have been paid intensive attention as potential electro-luminophore to replace the fluorescence, phosphorescence, and conventional TADF materials thanks to their unique characteristics such as high external quantum efficiency, narrow full-width half maximum (FWHM), and weak solvatochromism [2–8]. Since then, experimental and theoretical studies to extend the design space or identify the underlying spin-flip transition have been intensely reported [3,9–14]. However, in terms of theoretical approach, a proper methodology to predict the photo-physical properties of MR-TADF materials has been strongly desired since the conventional density functional theory (DFT) functionals known as the global, *meta*-GGA, and range-separated hybrid DFT functionals are inadequate to describe the nature of excited states in MR-TADF materials. Previously, Pershin et al., reported that Spin-Component Scaling second-order approximate Coupled Cluster (SCS-CC2) method can be successfully applied to quantitatively predict the energy difference between the lowest singlet (S_1) and triplet (T_1) states (ΔE_{ST}) of MR-TADF materials [15]. They noted that the correlation effect of wave-function method

* Corresponding author. Department of Materials Science and Engineering, Hongik University, Sejongsi, 30016, South Korea.
** Corresponding author.
E-mail addresses: sunwoo.kang@dankook.ac.kr (S. Kang), taekyung.kim@hongik.ac.kr (T. Kim).

https://doi.org/10.1016/j.heliyon.2024.e30926
Received 21 March 2024; Received in revised form 7 May 2024; Accepted 8 May 2024
Available online 11 May 2024

plays an essential role in accurately describing the double excitation characteristic of MR-TADF materials. Recently, Shizu and Kaji reported the important role of the equation-of-motion coupled-cluster single and double (EOM-CCSD) method in computing the accruate excited-state properties of DABNA-1 [16]. Moreover, the second-order algebraic diagrammatic contructiton (ADC(2)) and the spin-component scaling second-order algebraic diagrammatic contructiton (SCS-ADC(2)) were successfully utilized to describe the nature of excited states in MR-TADF materials [17]. Despite the advantage of these wave-function method in predicting the photo-physical properties of MR-TADF materials, the expensive time cost is a significant hurdle to use it conveniently. Accordingly, such a new approach, which should be simultaneously advantageous in terms of cheap time cost and excellent accuracy, is strongly desired. Recently, Pratic et al., reported that the similarity transformed EOM domain-based local pair natural orbital CCSD (STEOM-DLPNO-CCSD) [18] calculation at the optimized structures computed by optimally tuned time dependent (TD)-LC−⌉HPBE (TD-LC-⌉∗HPBE) accurately reproduces the experimentally determined photo-physical properties of several MR-TADF materials [19,20]. This result also supports that the considering the correlation effect is essentially required to describe the nature of both excited states in MR-TADF materials. Moreover, it has been known that STEOM-DLPNO-CCSD calculation was developed to reduce computing time while maintaining equivalent accuracy, compared to other wave-function methods. Therefore, we expect that TDDFT/STEOM-DLPNO-CCSD calculation could be utilized as one of alternative methodology to compute the excited-state properties of MR-TADF materials. However, it is further required to clarify that which DFT functional, combined with STEOM-DLPNO-CCSD, is the most advantageous to predict the photo-physical properties of MR-TADF materials. To address this question, we estimated the DFT functional that provides the superior quantitative prediction combined with STEOM-DLPNO-CCSD calculation. The conventionally used DFT functionals can be introduced as the global, *meta*-GGA, and range separated hybrid (RSH) functionals, respectively. Among them, B3LYP [21–23], M06 [24], LC-⌉∗HPBE [25–27] functionals were selected as representatives since these DFT functionals have been commonly utilized to investigate the excited-state properties in various type of chromophores. In the practical application, blue MR-TADF material with high internal quantum efficiency (IQE) has been received tremendous attentions to replace the current fluorescence emitter due to the limited exciton utilization efficiency. Therefore, the exact theoretical prediction of the excited-state properties to activate the virtual design of new blue MR-TADF materials are important to abundantly expand the design space and exactly understand the nature of excited-state properties. With this aim, we carefully selected 10 representative blue MR-TADF materials to estimate the prediction quality of theoretical methodologies in this study (See Fig. 1).

In this present works, we strongly ensure that our presented research importantly guides the appropriate computation approach to accurately obtain the excited-state properties of MR-TADF materials. Furthermore, we believe that our research may contribute to the understanding of the underlying mechanism as well as designing of the new materials in the MR-TADF materials.

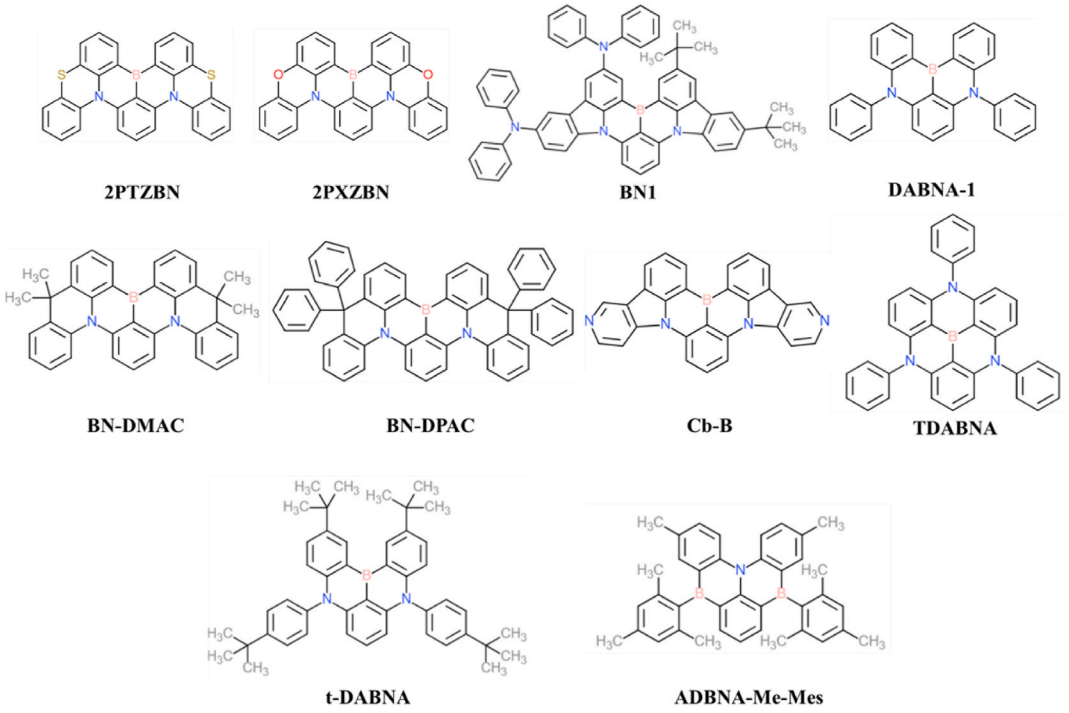

Fig. 1. The schematic structures of MR-TADF materials.

2. Theory and computation

DFT simulations for **2PTZBN** [28], **2PXZBN** [28], **BN1** [29], **DABNA-1** [1], **BN-DMAC** [30], **BN-DPAC** [30], **Cb-B** [14], **TABNA** [31], **t-DABNA** [32], and **ADBNA-Me-Mes** [33] were carried out employing B3LYP, M06, LC-ω*HPBE with 6-311G** basis sets, as implemented in the suite of Gaussian 16 package [34]. These materials were selected as represent materialsFor LC-ω*HPBE, the ω* (the optimal ω) can be determined at the minimum of $J^2(\omega)$ as a function of ω. This can be obtained by the following equation.

$$J^2(\omega) = \sum_{i=0}^{1} [\varepsilon_H(N+i) + IP(N+i)]^2 \quad (1)$$

where ε_H, N, IP indicate the energy level of the highest occupied molecular orbital, electron number of system, and ionization potential, respectively. The calculated ω* values for MR-TADF materials were listed in Table 1. At the optimized structures in the ground state (S_0), time-dependent DFT (TDDFT) calculations of the singlet and triplet excited-states (S_1 and T_1) in conjunction with Tamm-Dancoff Approximation (TDA) [35] were performed to obtain the optimized structures and their corresponding emission energies with same functional and basis set. All molecular structures of S_0, S_1, and T_1 states were optimized without any symmetry constraints (C1) in the gas phase. Moreover, frequency calculations for optimized structures of S_0, S_1, and T_1 states were conducted to confirm thermodynamic stability, showing that there is no imaginary in these optimized structures. To further consider the correlation effect for MR-TADF materials, STEOM-DLPNO-CCSD calculations at the optimized structures of S_1 and T_1 states computed by TDDFT calculations were further conducted, as implemented in the ORCA 5.0 program [36]. Def2-TZVP basis set and their corresponding auxiliary basis sets were used. In addition, RIJCOSX approximation was utilized to consider the acceleration of the SCF.

3. Results and discussions

3.1. 3-1. DFT calculations

The adiabatic excitation energies of the representative MR-TADF materials computed by B3LYP, M06, and LC-]*HPBE functionals are listed in Table 2. Moreover, the regression plots of S_1, T_1, and ΔE_{ST} between theory and experiment are depicted in Fig. 2. Interestingly, it is noticed that the qualitative predictions of S_1 and T_1 energies were successfully achieved with B3LYP, M06, and LC-]*HPBE functionals. Moreover, the qualitative predictions of S_1 and T_1 energies are superior in the order of LC-]*HPBE > M06 > B3LYP. This result indicates that B3LYP, M06, and LC-]*HPBE functionals can be utilized in the role of screening or categorizing the energies of both excited states in MR-TADF materials. On the contrary, the comparison of the ΔE_{ST} values in theory and experiment reveals that DFT functionals are inadequate to utilize as a qualitative prediction of the ΔE_{ST}.

Let us turn to see the quantitative perspective. As shown in Fig. 3(a), most of the calculated S_1 energies by B3LYP, M06, and LC-]*HPBE functionals are larger than the experimentally measured values. However, the calculated T_1 energies are generally underestimated except M06 functional. In addition, the calculated ΔE_{ST} values are significantly larger than the experimentally measured ones. To compare the quantitative prediction accuracy of these DFT functionals, the root means square error (RMSE) values of S_1, T_1, and ΔE_{ST} were derived. For the calculated S_1 energy, the RMSEs of LC-]*HPBE, B3LYP, and M06 functionals are 0.274, 0.132, and 0.284, showing higher accuracy in the order of B3LYP > LC-]*HPBE > M06. In contrast, the RMSEs of LC-]*HPBE, B3LYP, and M06 functionals for computed T_1 energies are 0.126, 0.167, and 0.087, determining higher accuracy in the order of M06 > LC-]*HPBE > B3LYP. Moreover, the RMSEs of the computed ΔE_{ST} for LC-]*HPBE, B3LYP, and M06 functionals are 0.355, 0.225, and 0.257, indicating the higher accuracy in the order of B3LYP > M06 > LC-]*HPBE. According to the RMSEs of S_1, T_1, and ΔE_{ST}, it can be understood that energy gaps between TDDFT calculations and experiments are remarkably large to use as the aim of the quantitative prediction. In addition to TDDFT calculations, we further considerd the ⊗ SCF method to calculate the T_1 energy since it has been

Table 1
The optimal].values for MR-TADF materials. The unit is in $Bohr^{-1}$.

	LC-]*HPBE
2PTZBN	0.159
2PXZBN	0.180
BN1	0.136
DABNA-1	0.170
BN-DPAC	0.141
BN-DMAC	0.155
Cb-B	0.170
TABNA	0.161
tDABNA	0.151
ADBNA-Me-Mes	0.156

Table 2
The calculated S_1, T_1, and ΔE_{ST} values by TDDFT calculations. All unit is in eV.

	LC-]*HPBE			B3LYP			M06			Exp.		
	S_1	T_1	ΔE_{ST}	S_1	T_1	ΔE_{ST}	S_1	T_1	ΔE_{ST}	S_1	T_1	ΔE_{ST}
2PTZBN	2.69	2.24	0.45	2.53	2.16	0.37	2.69	2.32	0.37	2.59	2.44	0.15
2PXZBN	2.83	2.28	0.55	2.50	2.14	0.36	2.73	2.31	0.42	2.60	2.41	0.19
BN1	2.64	2.20	0.44	2.48	2.2	0.28	2.74	2.34	0.40	2.50	2.39	0.11
DABNA-1	3.13	2.55	0.58	2.89	2.49	0.4	3.10	2.67	0.43	2.74	2.59	0.15
BN-DPAC	2.68	2.27	0.41	2.63	2.28	0.35	2.80	2.44	0.36	2.53	2.40	0.13
BN-DMAC	2.81	2.34	0.47	2.68	2.3	0.38	2.84	2.46	0.38	2.56	2.42	0.14
Cb-B	3.07	2.55	0.52	2.89	2.47	0.42	3.06	2.63	0.43	2.70	2.58	0.12
TABNA	3.58	2.94	0.64	3.36	2.94	0.42	3.55	3.09	0.46	3.11	2.90	0.21
tDABNA	2.99	2.45	0.54	2.88	2.45	0.43	3.04	2.60	0.44	2.80	2.63	0.17
ADBNA-Me-Mes	2.77	2.31	0.46	2.66	2.31	0.35	2.82	2.41	0.41	2.57	2.39	0.18
RMSE	0.274	0.126	0.355	0.132	0.167	0.225	0.284	0.087	0.257			

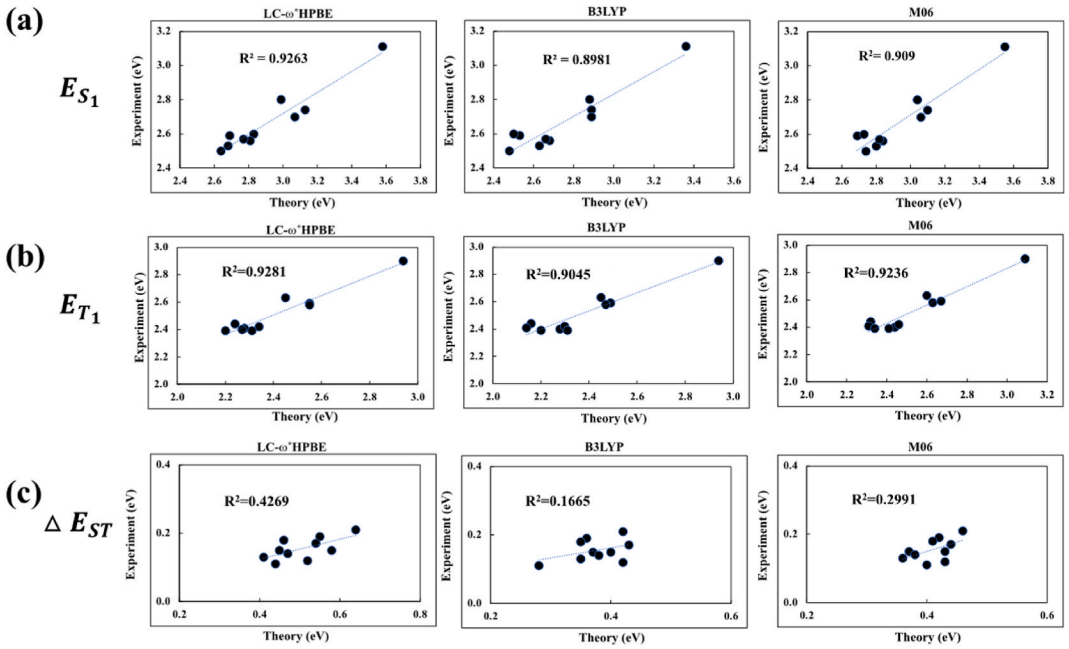

Fig. 2. The regression plots between TDDFT calculation and experiment (a) S_1 energy, (b) T_1 energy, and (c) ΔE_{ST}.

known as the efficient methodology to optimize the structure in T_1 state [37,38]. Specifically, ⊗ SCF calculations by LC-]*HPBE functional were conducted with the individual]* values of MR-TADF materials. Therefore, the computed T_1 energies were compared to the experiments and TDDFT calculations. As listed and shown in Table 3 and Fig. 3(b), it can be seen that T_1 energies computed by ⊗ SCF method are slightly larger than TDDFT calculations. More importantly, according to the RMSE values, ⊗ SCF calculations computed by LC-]*HPBE and B3LYP exhibit better quantitative T_1 energies than TDDFT calculations. On the other hand, M06 functional is disadvantageous to obtain the quantitative T_1 energy of MR-TADF material. We further compare $\otimes\bigoplus_{ST}$ values that derived from difference between S_1 (TDDFT) and T_1 (⊗ SCF) energies. As a result, it is noticed that ⊗ SCF calculation is more beneficial than TDDFT calculation in terms of the accurate $\otimes\bigoplus_{ST}$ value and inexpensive time cost. This result implies that ⊗ SCF method can be selected as the alternative methodology to predict quantitative T_1 energy of MR-TADF materials.

Although ⊗ SCF method guarantees the improvement of the quantitative prediction of T_1 and ΔE_{ST}, the accuracy of the computed $\otimes\bigoplus_{ST}$ values are not yet enough to accurately describe the spin-flip transition of MR-TADF. Consequently, these results make us to insist that TDDFT and ⊗ SCF calculations can inform incorrect parameters, leading to the misunderstanding of the spin-flip behavior of MR-TADF materials.

3.2. 3-2. STEOM-DLPNO-CCSD calculation

As mentioned in the introduction, the correlation effect must be considered to quantitatively calculate the energies of both excited

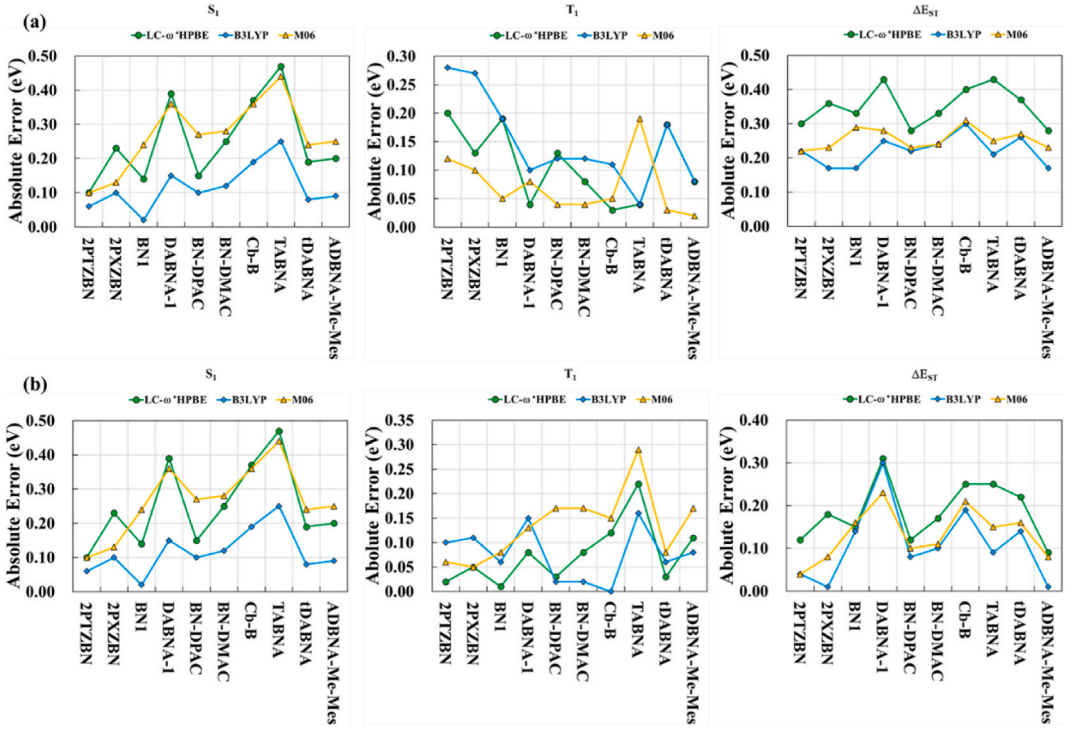

Fig. 3. The absolute errors of S_1, T_1, and ΔE_{ST} between DFT calculations and experiments. (a) TDDFT calculations (S_1 and T_1) (b) TDDFT (S_1) and ⊗ SCF (T_1) calculations.

Table 3
The calculated S_1, T_1, and ΔE_{ST} values by TDDFT (S_1) and ⊗ SCF (T_1) calculations. All unit is in eV.

	LC-ω*HPBE			B3LYP			M06			Exp.		
	S_1	T_1	ΔE_{ST}	S_1	T_1	ΔE_{ST}	S_1	T_1	ΔE_{ST}	S_1	T_1	ΔE_{ST}
2PTZBN	2.69	2.42	0.27	2.53	2.34	0.19	2.69	2.50	0.19	2.59	2.44	0.15
2PXZBN	2.83	2.46	0.37	2.50	2.30	0.20	2.73	2.46	0.27	2.60	2.41	0.19
BN1	2.64	2.38	0.26	2.48	2.33	0.25	2.74	2.47	0.27	2.50	2.39	0.11
DABNA-1	3.13	2.67	0.46	2.89	2.44	0.45	3.10	2.72	0.38	2.74	2.59	0.15
BN-DPAC	2.68	2.43	0.25	2.63	2.42	0.21	2.80	2.57	0.23	2.53	2.40	0.13
BN-DMAC	2.81	2.50	0.31	2.68	2.44	0.24	2.84	2.59	0.25	2.56	2.42	0.14
Cb-B	3.07	2.70	0.37	2.89	2.58	0.31	3.06	2.73	0.33	2.70	2.58	0.12
TABNA	3.58	3.12	0.46	3.36	3.06	0.30	3.55	3.19	0.36	3.11	2.90	0.21
tDABNA	2.99	2.60	0.39	2.88	2.57	0.31	3.04	2.71	0.33	2.80	2.63	0.17
ADBNA-Me-Mes	2.77	2.50	0.27	2.66	2.47	0.19	2.82	2.56	0.26	2.57	2.39	0.18
RMSE	0.274	0.096	0.198	0.132	0.092	0.132	0.284	0.151	0.144			

states in MR-TADF materials. Therefore, single-point STEOM-DLPNO-CCSD calculations were further conducted at the optimized geometries of TDDFT calculations. The calculated S_1, T_1, and ΔE_{ST} values are collected in Table 4. In addition, the regression plots of S_1, T_1, and ΔE_{ST} between theory and experiment are depicted in Fig. 4. According to the R^2, it is worth noticing for S_1 energy that TD-LC-ω*HPBE/STEOM-DLPNO-CCSD and TD-B3LYP/STEOM-DLPNO-CCSD calculations appear R^2 more than 0.8 while TD-M06/STEOM-DLPNO-CCSD calculation exhibits R^2 below than 0.5. Interestingly, all TDDFT/STEOM-DLPNO-CCSD calculations display R^2 more than 0.8 for T_1 energy. These results indicate the reliable quantitative prediction. Although TDDFT/STEOM-DLPNO-CCSD calculations are in qualitative agreement with experiments, we believe that the utilization of these methodologies as qualitative prediction seem to be less meaningful than DFT calculations. Because all data points of TDDFT/STEOM-DLPNO-CCSD calculations are more dispersive than those of DFT calculations, indicating the overestimation of R^2.

The energy gaps of S_1, T_1, and ΔE_{ST} between theory and experiment are depicted in Fig. 5, notifying that the calculated S_1, T_1, and ΔE_{ST} are close to the experiments. In detail, TD-LC-ω*HPBE/STEOM-DLPNO-CCSD calculations show the smallest RMSEs for S_1, T_1, and ΔE_{ST} (0.097, 0.084, and 0.058). On the other hand, TD-M06/STEOM-DLPNO-CCSD calculations exhibit the largest RMSEs in predicting the S_1, T_1, and ΔE_{ST} (0.157, 0.116, and 0.145). Therefore, it is obtained that the quantitative predictions are more accurate

Table 4
The calculated S_1, T_1, and ΔE_{ST} values by DFT coupled to STEOM-DLPNO-CCSD calculations. All unit is in eV.

	LC-]*HPBE			B3LYP			M06			Exp.		
	S_1	T_1	ΔE_{ST}	S_1	T_1	ΔE_{ST}	S_1	T_1	ΔE_{ST}	S_1	T_1	ΔE_{ST}
2PTZBN	2.57	2.45	0.12	2.65	2.44	0.21	2.58	2.36	0.22	2.59	2.44	0.15
2PXZBN	2.63	2.39	0.24	2.62	2.39	0.23	2.64	2.32	0.32	2.60	2.41	0.19
BN1	2.60	2.39	0.21	2.78	2.42	0.36	2.75	2.51	0.24	2.50	2.39	0.11
DABNA-1	2.88	2.69	0.19	2.88	2.70	0.18	2.92	2.75	0.17	2.74	2.59	0.15
BN-DPAC	2.59	2.4	0.19	2.71	2.62	0.09	2.67	2.51	0.16	2.53	2.40	0.13
BN-DMAC	2.65	2.42	0.23	2.66	2.50	0.16	2.70	2.51	0.19	2.56	2.42	0.14
Cb-B	2.87	2.79	0.08	2.88	2.69	0.19	2.92	2.72	0.20	2.70	2.58	0.12
TABNA	3.21	2.93	0.28	3.30	3.04	0.26	2.91	3.09	−0.18	3.11	2.90	0.21
tDABNA	2.74	2.57	0.17	2.84	2.66	0.18	2.88	2.69	0.19	2.80	2.63	0.17
ADBNA-Me-Mes	2.67	2.50	0.17	2.66	2.50	0.16	2.69	2.41	0.18	2.57	2.39	0.18
RMSE	0.097	0.084	0.058	0.149	0.106	0.089	0.157	0.116	0.145			

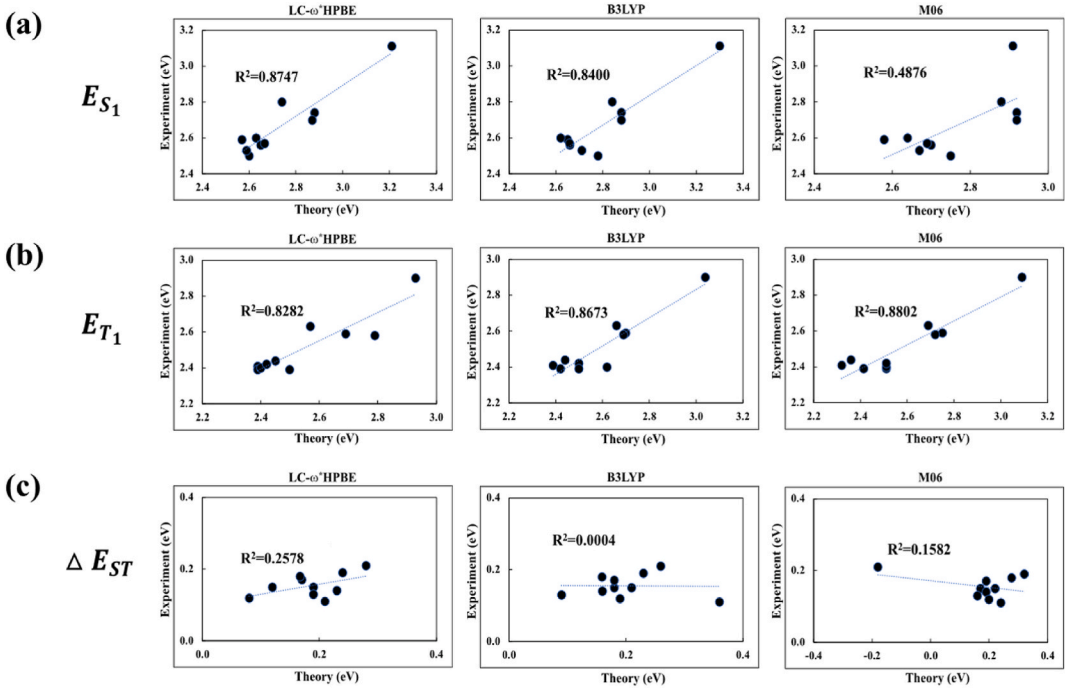

Fig. 4. The regression plots between DFT/STEOM-DLPNO-CCSD calculations and experiments. (a) S_1 energy (b) T_1 energy (c) ⊗ E_{ST}.

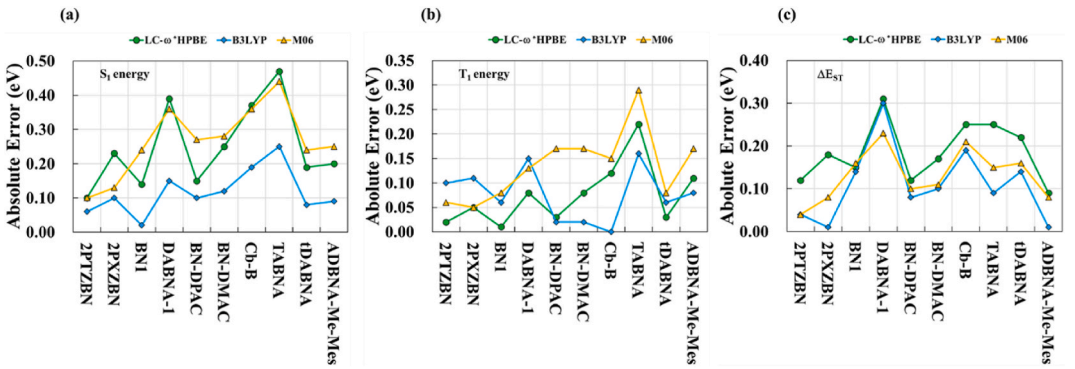

Fig. 5. The absolute errors between DFT/STEOM-DLPNO-CCSD calculations and experiments. (a) S_1 energy (b) T_1 energy (c) ΔE_{ST}.

in the order of TD-LC-]*HPBE/STEOM-DLPNO-CCSD > TD-B3LYP/STEOM-DLPNO-CCSD > TD-M06/STEOM-DLPNO-CCSD calculations. This result confirms the superior performance of TD-LC-]*HPBE/STEOM-DLPNO-CCSD calculation in predicting the excited state properties of MR-TADF materials. Subsequently, this also clarifies the essential role of TDDFT/STEOM-DLPNO-CCSD calculation in understanding the spin-flip transition of MR-TADF materials. Nonetheless, it is worthy noticing that TD-M06/STEOM-DLPNO-CCSD calculation shows the larger RMSE for T_1 energy, compared to TD-M06 calculation. More surprisingly, TD-M06/STEOM-DLPNO-CCSD calculation for **TABNA** gives an unexpected negative ΔE_{ST}, which incorrectly reproduced the experimental value. This abnormal result will be discussed and analyzed by further computation in a later study. Although TD-M06/STEOM-DLPNO-CCSD calculation exhibits the disadvantageous point, TDDFT/STEOM-DLPNO-CCSD calculation clearly shows the remarkable advantages over TDDFT calculation in understanding the excited states properties of MR-TADF materials. Nonetheless, compared to TD-LC-]*HPBE/STEOM-DLPNO-CCSD and TD-B3LYP/STEOM-DLPNO-CCSD calculations, TD-M06/STEOM-DLPNO-CCSD calculation seems to be inadequate to quantitatively compute the S_1, T_1, and ΔE_{ST} of MR-TADF materials. Therefore, TD-LC-]*HPBE/STEOM-DLPNO-CCSD and TD-B3LYP/STEOM-DLPNO-CCSD calculations are suggested to meaningfully predict the photo-physical properties of MR-TADF materials. Specifically, TD-LC-]*HPBE/STEOM-DLPNO-CCSD calculation must be primarily considered to investigate the excited-state properties of MR-TADF materials.

In conclusion, we can strongly propose that TD-LC-]*HPBE/STEOM-DLPNO-CCSD calculation should be utilized as the efficient and powerful methodology to accurately calculate the pivotal excited-state properties of MR-TADF materials.

4. Conclusion

TDDFT and TDDFT/STEOM-DLPNO-CCSD calculations were comparably studied to key parameters of excited states in MR-TADF materials. Similar to previous reports, it was clarified that TDDFT calculations based on B3LYP, M06, and LC-]*HPBE functionals are obviously inadequate to quantitatively compute the S_1, T_1, and ΔE_{ST} of MR-TADF materials. Nevertheless, TDDFT calculation can be utilized as a screening tool to qualitatively predict the photo-physical properties of MR-TADF materials. On the contrary, these parameters can be quantitatively predicted based on TDDFT/STEOM-DLPNO-CCSD calculation. More specifically, TD-LC-]*HPBE/STEOM-DLPNO-CCSD calculation gives the most superior quantitative prediction. Therefore, we propose that LC-]*HPBE/DLPNO-STEOM-CCSD calculation should be used to describe the exact nature of the excited states of MR-TADF materials.

CRediT authorship contribution statement

Sunwoo Kang: Writing – review & editing, Writing – original draft, Supervision, Formal analysis, Data curation, Conceptualization. **Taekyung Kim:** Writing – review & editing, Supervision.

Declaration of competing interest

There are no conflicts of interest to declare.

Acknowledgement

The present research was supported by the research fund of Dankook University in 2024.

References

[1] T. Hatakeyama, K. Shiren, K. Nakajima, S. Nomura, S. Nakatsuka, K. Kinoshita, J. Ni, Y. Ono, T. Ikuta, Ultrapure blue thermally activated delayed fluorescence molecules: efficient HOMO–LUMO separation by the multiple resonance effect, Adv. Mater. 28 (14) (2016) 2777–2781.
[2] X. Cai, J. Xue, C. Li, B. Liang, A. Ying, Y. Tan, S. Gong, Y. Wang, Achieving 37.1% Green Electroluminescent Efficiency and 0, 09 eV full width at half maximum based on a Ternary boron-Oxygen-Nitrogen Embedded Polycyclic Aromatic system, Angew. Chem. Int. Ed. 61 (23) (2022) e202200337.
[3] S. Oda, B. Kawakami, Y. Yamasaki, R. Matsumoto, M. Yoshioka, D. Fukushima, S. Nakatsuka, T. Hatakeyama, One-shot synthesis of expanded heterohelicene exhibiting narrowband thermally activated delayed fluorescence, J. Am. Chem. Soc. 144 (1) (2021) 106–112.
[4] S. Oda, B. Kawakami, M. Horiuchi, Y. Yamasaki, R. Kawasumi, T. Hatakeyama, Ultra-Narrowband blue multi-resonance thermally activated delayed fluorescence materials, Adv. Sci. 10 (1) (2023) 2205070.
[5] Y. Kondo, K. Yoshiura, S. Kitera, H. Nishi, S. Oda, H. Gotoh, Y. Sasada, M. Yanai, T. Hatakeyama, Narrowband deep-blue organic light-emitting diode featuring an organoboron-based emitter, Nat. Photonics 13 (10) (2019) 678–682.
[6] C. Prentice, J. Morrison, A.D. Smith, E. Zysman-Colman, Multi-resonant thermally activated delayed fluorescent (MR-TADF) Compounds as Photocatalysts, Chem.–Eur. J. 29 (2) (2023) e202202998.
[7] X.F. Luo, H.X. Ni, H.L. Ma, Z.Z. Qu, J. Wang, Y.X. Zheng, J.L. Zuo, Fused π-Extended multiple-resonance induced thermally activated delayed fluorescence materials for high-efficiency and narrowband OLEDs with Low efficiency Roll-Off, Adv. Opt. Mater. 10 (9) (2022) 2102513.
[8] J. Han, Z. Huang, X. Lv, J. Miao, Y. Qiu, X. Cao, C. Yang, Simple molecular design strategy for multiresonance induced TADF emitter: highly efficient deep blue to blue electroluminescence with high color purity, Adv. Opt. Mater. 10 (4) (2022) 2102092.
[9] Y. Liu, X. Xiao, Z. Huang, D. Yang, D. Ma, J. Liu, B. Lei, Z. Bin, J. You, Space-confined Donor-Acceptor strategy Enables fast spin-flip of multiple resonance emitters for Suppressing efficiency Roll-Off, Angew. Chem. 134 (40) (2022) e202210210.
[10] I. Kim, K.H. Cho, S.O. Jeon, W.-J. Son, D. Kim, Y.M. Rhee, I. Jang, H. Choi, D.S. Kim, Three states involving vibronic resonance is a key to enhancing reverse intersystem crossing dynamics of an organoboron-based ultrapure blue emitter, JACS Au 1 (7) (2021) 987–997.

[11] J. Jin, C. Duan, H. Jiang, P. Tao, H. Xu, W.Y. Wong, Integrating Asymmetric O– B– N Unit in multi-resonance thermally activated delayed fluorescence emitters towards high-performance deep-blue organic light-emitting Diodes, Angew. Chem. Int. Ed. 62 (18) (2023) e202218947.
[12] D. Hall, J.C. Sancho-García, A. Pershin, G. Ricci, D. Beljonne, E. Zysman-Colman, Y. Olivier, Modeling of multiresonant thermally activated delayed fluorescence Emitters— properly Accounting for electron correlation is key, J. Chem. Theor. Comput. 18 (8) (2022) 4903–4918.
[13] I.S. Park, H. Min, T. Yasuda, Ultrafast triplet–singlet exciton Interconversion in narrowband blue organoboron emitters Doped with Heavy Chalcogens, Angew. Chem. Int. Ed. 61 (31) (2022) e202205684.
[14] M. Yang, S. Shikita, H. Min, I.S. Park, H. Shibata, N. Amanokura, T. Yasuda, Wide-range color tuning of narrowband emission in multi-resonance organoboron delayed fluorescence materials through Rational Imine/Amine Functionalization, Angew. Chem. Int. Ed. 60 (43) (2021) 23142–23147.
[15] A. Pershin, D. Hall, V. Lemaur, J.-C. Sancho-Garcia, L. Muccioli, E. Zysman-Colman, D. Beljonne, Y. Olivier, Highly emissive excitons with reduced exchange energy in thermally activated delayed fluorescent molecules, Nat. Commun. 10 (1) (2019) 597.
[16] K. Shizu, H. Kaji, Comprehensive understanding of multiple resonance thermally activated delayed fluorescence through quantum chemistry calculations, Commun. Chem. 5 (1) (2022) 53.
[17] A. Tajti, B. Kozma, P.G. Szalay, Improved description of charge-transfer potential energy surfaces via spin-component-scaled CC2 and ADC (2) methods, J. Chem. Theor. Comput. 17 (1) (2020) 439–449.
[18] R. Berraud-Pache, F. Neese, G. Bistoni, R. Izsák, Unveiling the photophysical properties of boron-dipyrromethene dyes using a new accurate excited state coupled cluster method, J. Chem. Theor. Comput. 16 (1) (2019) 564–575.
[19] S.M. Pratik, V. Coropceanu, J.-L. Brédas, Purely organic emitters for multiresonant thermally activated delay fluorescence: design of highly efficient sulfur and selenium derivatives, ACS Mater. Lett. 4 (3) (2022) 440–447.
[20] S.M. Pratik, V. Coropceanu, J.-L. Brédas, Enhancement of thermally activated delayed fluorescence (TADF) in multi-resonant emitters via control of chalcogen atom embedding, Chem. Mater. 34 (17) (2022) 8022–8030.
[21] A.D. Becke, Density-functional exchange-energy approximation with correct asymptotic behavior, Physical review A 38 (6) (1988) 3098.
[22] C. Lee, W. Yang, R.G. Parr, Development of the Colle-Salvetti correlation-energy formula into a functional of the electron density, Physical review B 37 (2) (1988) 785.
[23] A.D. Becke, A new inhomogeneity parameter in density-functional theory, The Journal of chemical physics 109 (6) (1998) 2092–2098.
[24] Y. Zhao, D.G. Truhlar, The M06 suite of density functionals for main group thermochemistry, thermochemical kinetics, noncovalent interactions, excited states, and transition elements: two new functionals and systematic testing of four M06-class functionals and 12 other functionals, Theor. Chem. Acc. 120 (2008) 215–241.
[25] O.A. Vydrov, G.E. Scuseria, Assessment of a long-range corrected hybrid functional, The Journal of chemical physics 125 (23) (2006).
[26] O.A. Vydrov, J. Heyd, A.V. Krukau, G.E. Scuseria, Importance of short-range versus long-range Hartree-Fock exchange for the performance of hybrid density functionals, The Journal of chemical physics 125 (7) (2006).
[27] O.A. Vydrov, G.E. Scuseria, J.P. Perdew, Tests of functionals for systems with fractional electron number, The Journal of chemical physics 126 (15) (2007).
[28] T. Hua, L. Zhan, N. Li, Z. Huang, X. Cao, Z. Xiao, S. Gong, C. Zhou, C. Zhong, C. Yang, Heavy-atom effect promotes multi-resonance thermally activated delayed fluorescence, Chem. Eng. J. 426 (2021) 131169.
[29] Y. Qi, W. Ning, Y. Zou, X. Cao, S. Gong, C. Yang, Peripheral decoration of multi-resonance molecules as a versatile approach for simultaneous long-wavelength and narrowband emission, Adv. Funct. Mater. 31 (29) (2021) 2102017.
[30] P. Jiang, L. Zhan, X. Cao, X. Lv, S. Gong, Z. Chen, C. Zhou, Z. Huang, F. Ni, Y. Zou, Simple Acridan-based multi-resonance structures enable highly efficient narrowband Green TADF electroluminescence, Adv. Opt. Mater. 9 (21) (2021) 2100825.
[31] S. Nakatsuka, H. Gotoh, K. Kinoshita, N. Yasuda, T. Hatakeyama, Divergent synthesis of Heteroatom-Centered 4, 8, 12-Triazatriangulenes, Angew. Chem. 129 (18) (2017) 5169–5172.
[32] S.H. Han, J.H. Jeong, J.W. Yoo, J.Y. Lee, Ideal blue thermally activated delayed fluorescence emission assisted by a thermally activated delayed fluorescence assistant dopant through a fast reverse intersystem crossing mediated cascade energy transfer process, J. Mater. Chem. C 7 (10) (2019) 3082–3089.
[33] S. Oda, B. Kawakami, R. Kawasumi, R. Okita, T. Hatakeyama, Multiple resonance effect-induced sky-blue thermally activated delayed fluorescence with a narrow emission band, Org. Lett. 21 (23) (2019) 9311–9314.
[34] M. Frisch, G. Trucks, H.B. Schlegel, G. Scuseria, M. Robb, J. Cheeseman, G. Scalmani, V. Barone, G. Petersson, H. Nakatsuji, Gaussian 16, Gaussian, Inc., Wallingford, CT, 2016.
[35] A.L. Fetter, J. Walecka, Theory of Many-Particle Systems, McGraw Hill, New York, 1971.
[36] F. Neese, Software update: the ORCA program system—Version 5.0, Wiley Interdiscip. Rev. Comput. Mol. Sci. 12 (5) (2022) e1606.
[37] S. Kang, T. Kim, Insight into understanding the photo-chemical stability of bis-tridentate Ir(III) phosphors: a theoretical perspective, Dyes and Pigm 201 (2022) 110191.
[38] S. Kang, T. Kim, J.Y. Lee, New design strategy for chemically-stable blue phosphorescent materials: improving the energy gap between the T1 and 3MC states, Phy, Chem. Chem. Phy. 5 (2021) 3543–3551.